Temperature Stabilization of the Phase-Reference Line at the European Spallation Source

Olofsson, Bjorn; Bernhardsson, Bo; Zeng, Rihua; Andersson, Pontus; Johansson, Rolf

Published in:
2018 IEEE Conference on Control Technology and Applications, CCTA 2018

DOI:
10.1109/CCTA.2018.8511364

2018

Document Version:
Peer reviewed version (aka post-print)

Temperature Stabilization of the Phase-Reference Line at the European Spallation Source

Björn Olofsson[1], Bo Bernhardsson[1], Rihua Zeng[2], Pontus Andersson[1], and Rolf Johansson[1]

***Abstract*— We consider temperature stabilization of the phase-reference line at the European Spallation Source, a facility for neutron spallation currently under construction. Based on extensive modeling of the heat dynamics, a prototype model-based control system with associated hardware architecture is developed and experimentally evaluated on a small-scale setup. The results indicate that temperature stability within ± 0.1 °C is possible to achieve, also with significant disturbances in the ambient temperature expected during operation.**

I. Background and Introduction

The European Spallation Source (ESS) is a facility for neutron spallation under construction in Lund, Sweden [1]. Protons are accelerated in an approx. 600 m accelerator, whereby they are collided with a tungsten target and neutrons are emitted. The neutrons are to be used in various experiments [1], with expected applications in areas such as material science, medical and life science, and pharmacology.

The protons are accelerated using electro-magnetic fields in so called cavities, which are connected in series to form the complete accelerator. To provide each proton-accelerating component in the accelerator with a stable reference time, such that the acceleration can be performed at the correct time instant, an ultra-stable clock is used as a master reference. The phase reference to each component is then transported along the accelerator as an analog signal in a rigid coaxial line [2], referred to as the phase-reference line. The accelerator includes in total 155 different accelerating components, of which some are superconducting [1]. The phase reference will also be used in all diagnostic systems for the accelerating proton beam. This fact requires both low phase noise and low phase drift in the reference signal. Thus, the phase-reference distribution system is an essential component for ESS in order to achieve the desired velocity and uniformity of the beam of protons when reaching the target, where the spallation of neutrons takes place. The radio-frequency wave that constitutes the phase reference is transported in a rigid coaxial line made of copper [2], with one inner and one outer conductor, see Fig. 1. In addition to the rigid coaxial line, the phase-reference distribution system at ESS consists of directional couplers and splitters connected approximately each 10 m for extracting the phase information for each cavity in the accelerator.

*The research presented was co-financed by the European Spallation Source ERIC. All authors except R. Zeng are members of the ELLIIT Strategic Research Area, supported by the Swedish Government, and the LCCC Linnaeus Center, supported by the Swedish Research Council.

[1]Department of Automatic Control, Lund University, Lund, Sweden. E-mail: bjorn.olofsson@control.lth.se.

[2]European Spallation Source ERIC, Lund, Sweden.

Fig. 1. Rigid coaxial line with directional coupler (to the right) used in the phase-reference distribution system at ESS. Sensors for surface measurements of the temperature and a heating cable wound around the outer copper tube have been mounted on the coaxial line. The complete phase-reference line and directional couplers are then insulated (see Fig. 7).

This paper presents the development and experimental evaluation of a prototype temperature stabilization control system for the phase-reference line at ESS. The stabilization is based on feedback control from measurements of the surface temperature of the copper coaxial line. Moreover, heating cables are wound around the phase-reference line and then insulation is applied (Fig. 1). A developed small-scale phase-reference line of approximate length 5 m (Fig. 6) was used for the experimental evaluations in this paper. Both simulation and experimental results are presented, highlighting the characteristics and performance of the system. Related research on feedback-based control systems for temperature stabilization of phase-reference lines in accelerators, employing temperature measurements and heating elements, has been presented previously in [3]. The main contributions of the current paper are an extensive analytical modeling of the system dynamics considered, a completely model-based control design, as well as a control-hardware architecture for robust integration with the central accelerator control system to be used at ESS. Results, without detailed derivation and description of the analytical modeling and the model-based control design, for parts of the research presented in the current paper were described in the poster [4].

II. Problem Formulation

A major control challenge for the phase-reference distribution system at ESS is that the long-term phase drift must be less than 1 deg. (corresponding to approximately 4 ps at the target frequency of 704.42 MHz) for any two different locations along the linear accelerator. Considering that the phase reference is distributed along a rigid coaxial line made of copper, unavoidable temperature variations in the accelerator tunnel during operation will induce length

variations of the copper conductors forming the rigid line, leading to undesirable phase changes at the tap points at each cavity. The length coefficient of copper is approximately 17 ppm/°C. The allowed phase variations, wave frequency, and the total length of the phase-reference line determine the temperature stability required. The phase-reference system is calibrated in a certain state, *i.e.*, each point along the phase-reference line has a certain temperature (though not necessarily the same temperature for all points). Variations from the calibrated temperature during operation of the accelerator can thus induce phase variations. Assuming a linear coordinate x along the phase-reference line, the phase change $\Delta\varphi$ between points x_0 and x_f at time t exhibits a proportional relationship with temperature variations according to

$$\Delta\varphi \sim \int_{x_0}^{x_f} T(x,t) - T_{\mathrm{cal}}(x)\ \mathrm{d}x, \tag{1}$$

where T and T_{cal} are the current temperature and the temperature at calibration, respectively. Both of these quantities depend on the coordinate along the phase-reference line. The intuitive interpretation of this relation is that positive and negative temperature changes average out, whereas, *e.g.*, only positive temperature changes lead to phase variations. A simplified, and in some cases conservative, temperature-stability requirement provided by ESS for the prototype setup discussed in this paper is to achieve

$$\max_{x,t} |T(x,t) - T_{\mathrm{cal}}(x)| \leq 0.1\ ^{\circ}\mathrm{C}, \tag{2}$$

where T_{cal} in the experimental evaluations is interpreted as the temperature at the start of the experiment. In this context, it is to be noted that different parts of the phase-reference line will have different temperatures at the calibration time.

III. Modeling

This section presents the fundamentals of the heat-transfer modeling and defines the models employed as a basis for the control design and architecture presented in Secs. IV–V.

A. Heat-Transfer Modeling

The partial differential equation (PDE) governing the heat diffusion in three dimensions is given by [5]

$$\nabla \cdot (k\nabla T) + Q = \rho c T'_t, \tag{3}$$

where k is thermal conductivity, T temperature, Q internal heat generation, ρ density, and c specific heat capacity.

At the boundary between an object and the environment, *e.g.*, between the insulation of the phase-reference line and the surrounding air, heat flow will occur. This dynamic relation is modeled using convection, which mathematically could be stated as [5]

$$q = h(T - T_{\mathrm{air}}), \tag{4}$$

where q is the heat flow, T_{air} the temperature of the ambient air, and h is the heat-transfer coefficient. The parameters for the different materials to be considered for the phase-reference line are the density ρ (kg/m^3), the specific heat capacity c (J/(kg·K)), and the thermal conductivity k (W/(m·K)). The nominal values of these parameters for the materials of interest are provided in Table I. The heat-transfer coefficient h depends on the surface geometry and the air velocity and the heat flow increases with the air velocity. The parameter h depends on, *e.g.*, the ventilation and the mounting, but was found to have low impact on the simulation results. Numerical values in the considered application are in the range $h \in [5, 20]$ W/(m^2·K).

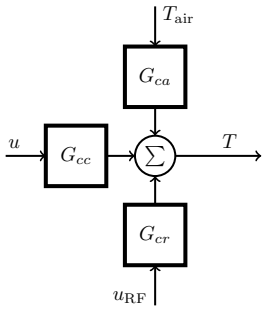

Fig. 2. Block diagram of the system with associated disturbances.

B. Block Diagram of the Process Dynamics

The block diagram of the phase-reference line system and associated disturbances is shown in Fig. 2. The temperature of the outer tube of the coaxial line is denoted T (assumed to be measured directly on the surface, see Fig. 1). The air temperature is denoted T_{air}. The heat applied by the controller through the heating cables is u, whereas u_{RF} is the heat losses in the coaxial line because of natural damping of radio-frequency (RF) waves in a copper coaxial line. The control objective is to stabilize T, despite disturbances in T_{air} and u_{RF} by manipulating the input u (with the additional constraint that $u \geq 0$). In order to keep the coaxial line free from moisture during operation, compressed air will be applied inside the outer copper tube at one end of it. Since the system is almost closed, however, the resulting airflow dynamics can be considered quasi-static and will therefore be neglected in the simulations of the temperature distribution.

The dynamics of the subsystems in Fig. 2 were investigated using both analytic and numerical methods. An analytical analysis was performed, and subsequently an extensive simulation study using a computer tool based on the finite-element method (FEM) was executed. Transfer functions for the subsystems G_{cc} and G_{ca} in Fig. 2 are estimated in Sec. VI.

C. Stationary Temperature Distribution

In this section, the stationary temperature distribution in a cross section of the phase-reference line (with insulation

TABLE I

Nominal values of the thermal properties for the materials.

Material	ρ **[kg/m^3]**	c **[J/(kg·K)]**	k **[W/(m·K)]**
Copper	8700	385	400
Aluminium	2700	1000	238
Insulation	100	1000	0.045

mounted around the outer copper tube) is computed. It is assumed that there are two heat sources Q^i and Q^o in the inner and outer copper tubes, respectively. The heat Q^i is generated because of RF wave losses in the copper conductors and Q^o is a combination of heat losses and applied heat from the heating cables. In the analysis in this subsection, the applied heat using the cables is assumed to be zero. Data from the manufacturer of the rigid line specify that $Q^i + Q^o$ is approximately 0.38 W/m in the beginning of the line and approximately 0.13 W/m in the end. The thermal conductivity properties for the respective material in a radial cross section are assumed to be as follows:

$$k = \begin{cases} k_{\text{air}}, & \text{air, } 0 < r \le r_1 \\ \infty, & \text{copper, } r_1 < r \le r_2 \\ k_{\text{air}}, & \text{air, } r_2 < r \le r_3 \\ \infty, & \text{copper, } r_3 < r \le r_4 \\ k_{\text{ins}}, & \text{insulation, } r_4 < r \le r_5 \end{cases} \tag{5}$$

The approximation with $k = \infty$ in the copper sections is here justified since it simplifies the computations, only at the price of a negligible error. A principal drawing of the cylindrical cross section of the phase-reference line is shown in Fig. 3 and the radial cross section is illustrated in Fig. 4.

Using the radial symmetry, the stationarity with respect to time, and that k is constant in each region i, the PDE (3) can be rewritten to the Laplace equation in cylinder coordinates (see, *e.g.*, [6]):

$$T''_{rr} + \frac{1}{r} T'_r = 0. \tag{6}$$

This relation gives the functions $T^i(r) = a_i + b_i \log(r)$ in region i with some constants a_i, b_i to be determined by the boundary conditions. The following expression is obtained

$$T(r) = \begin{cases} T^2, & 0 < r \le r_1 \\ T^2, & r_1 < r \le r_2 \\ T^2 + b_3 \log(\frac{r_2}{r}), & r_2 < r \le r_3 \\ T^4, & r_3 < r \le r_4 \\ T^4 + b_5 \log(\frac{r_4}{r}), & r_4 < r \le r_5 \end{cases} \tag{7}$$

At the inner copper conductor, the boundary condition is

$$Q^i = -2\pi r_2 k_{\text{air}} T'_r(r_2^+) = 2\pi k_{\text{air}} b_3, \tag{8}$$

from which it is obtained that $b_3 = Q^i/(2\pi k_{\text{air}})$. At the outer copper conductor, it holds that

$$Q^o = 2\pi r_3 k_{\text{air}} T'_r(r_3) - 2\pi r_4 k_{\text{ins}} T'_r(r_4^+), \tag{9}$$

which gives $b_5 = (Q^i + Q^o)/(2\pi k_{\text{ins}})$. The boundary condition at the outside of the insulation is, if it is normalized such that $T_{\text{air}} = 0$,

$$k T'_r(r_5) = -h T(r_5), \tag{10}$$

which gives

$$\frac{Q^i + Q^o}{2\pi r_5} = h \left(T^d + \frac{Q^i + Q^o}{2\pi k_{\text{ins}}} \log\left(\frac{r_4}{r_5}\right) \right), \tag{11}$$

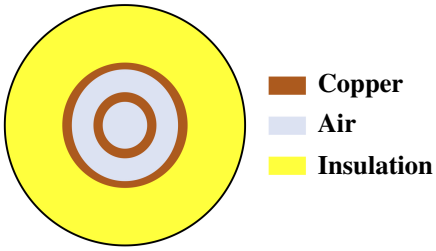

Fig. 3. Cylindrical cross section of the phase-reference line.

and

$$T^4 = \frac{Q^i + Q^o}{2\pi r_5} \left(\frac{1}{h} + \frac{r_5 \log\left(\frac{r_5}{r_4}\right)}{k_{\text{ins}}} \right). \tag{12}$$

It is interesting to note that T^4 only depends on $h, r_4, r_5, k_{\text{ins}}$, and $Q^i + Q^o$. Note also that it is the temperature T^4 that determines the length extension of the copper coaxial line and is therefore the interesting temperature in the cross section. Solving for T^2 gives

$$T^2 = T^4 + \frac{Q^i}{2\pi} \frac{\log\left(\frac{r_3}{r_2}\right)}{k_{\text{air}}}. \tag{13}$$

Based on the geometry of the phase-reference line, numerical parameters were introduced as

$$(r_1, r_2, r_3, r_4, r_5) = (7.5, 8.45, 19.4, 20.65, 60.65) \cdot 10^{-3} \text{ m}.$$

Under the assumption that the RF copper heat losses are $Q^i + Q^o = 0.38$ W/m and $h = 5$ W/(m^2·K), it follows that $T^4 = 1.83$. The temperature on the inner copper is $T^2 \in [1.83, 3.74]$, depending on the ratio $Q^i/(Q^i + Q^o)$.

D. Transient Temperature Analysis

The transient temperature response to a step disturbance in the ambient temperature T_{air} in a cross section of the phase-reference line is analyzed. The results from the analysis can be used for feedforward control design from measured air temperature, if it should be required. Transformation of the PDE (3) into cylindrical coordinates and employing the symmetry of the problem to be solved gives the relation

$$rc(r) T'_t = \frac{\partial}{\partial r} \left(r k(r) T'_r \right), \tag{14}$$

where $T(t, r)$ is the temperature at time t at radius r, $c(r)$ is the volumetric heat capacity in J/(m^3·K) as function of r, and $k(r)$ is the thermal conductivity in W/(m·K) as function of r. The heat-flux density in the unit W/m^2 is given by $q(t, r) = -k(r) T'_r$, see [5]. Considering the fact that the

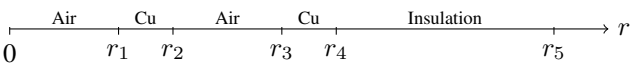

Fig. 4. Radial cross section of the phase-reference line, used to the purpose of analytic modeling of the heat transfer. Compare with Fig. 3.

temperature must be continuously changing in the phase-reference line, the following two conditions are necessary:

$$T \text{ and } -kT_r' \text{ are continuous functions of } r, \tag{15}$$

$$-k(r)T_r' = h(T - T_{\text{air}}) = hT, \text{ for } r = r_5, \tag{16}$$

where the last equality holds under the assumption that $T_{\text{air}} = 0$. The solution to the PDE (14) is computed using the principle of separation of variables and is written as[1]

$$T(t,r) = \sum_n d_n e^{-\lambda_n^2 t} T_n(r), \tag{17}$$

where the eigenvalues λ_n are defined by

$$\mathcal{A}T_n = \lambda_n^2 T_n, \tag{18}$$

with the Sturm-Liouville operator $\mathcal{A}$ (see [6]) defined as

$$\mathcal{A}y := -\frac{1}{rc(r)}\frac{\mathrm{d}}{\mathrm{d}r}\left(rk(r)\frac{\mathrm{d}y}{\mathrm{d}r}\right). \tag{19}$$

The operator $\mathcal{A}$ is self-adjoint in the domain

$$\mathcal{D}(\mathcal{A}) = \{y(r) : y(r) \text{ and } k(r)y'(r) \text{ are continuous and } -k(R)y'(R) = hy(R)\}, \tag{20}$$

where $R = r_5$ and the inner product is defined as

$$\langle f, g\rangle = \int_0^R f(r)g(r)rc(r)\mathrm{d}r. \tag{21}$$

In region i it holds that

$$\mathcal{A}T_{i,n} = -\frac{k_i}{c_i}\left(T_{i,n}'' + \frac{1}{r}T_{i,n}'\right), \tag{22}$$

and the equation $\mathcal{A}T_{i,n} = \lambda_n^2 T_{i,n}$ is there described by the Bessel equation

$$T_{i,n}'' + \frac{1}{r}T_{i,n}' + \mu_{i,n}^2 T_{i,n} = 0, \qquad \mu_{i,n}^2 := \frac{c_i}{k_i}\lambda_n^2, \tag{23}$$

which has the solution

$$T_{i,n}(r) = a_{i,n}J_0(\mu_{i,n}r) + b_{i,n}Y_0(\mu_{i,n}r), \tag{24}$$

for some real constants $a_{i,n}$, $b_{i,n}$, where J_0 and Y_0 are the Bessel functions of the first and second kind[2], respectively. The heat-flux density in region i is consequently given by

$$q_{i,n}(r) = -k_i T_{i,n}'(r) = a_{i,n}k_i\mu_{i,n}J_1(\mu_{i,n}r) + b_{i,n}k_i\mu_{i,n}Y_1(\mu_{i,n}r), \tag{25}$$

where J_1 and Y_1 are the derivatives of the Bessel functions of first and second kind, respectively. To simplify notation, the matrices

$$G_{i,n}(r) := \begin{bmatrix} J_0(\mu_{i,n}r) & Y_0(\mu_{i,n}r) \\ k_i\mu_{i,n}J_1(\mu_{i,n}r) & k_i\mu_{i,n}Y_1(\mu_{i,n}r)\end{bmatrix}, \tag{26}$$

are introduced. The solution in region i for eigenfunction n is hence given by

$$\begin{bmatrix} T_{i,n}(r) \\ q_{i,n}(r)\end{bmatrix} = G_{i,n}(r)x_{i,n}, \quad \text{where } x_{i,n} := \begin{bmatrix} a_{i,n} \\ b_{i,n}\end{bmatrix}. \tag{27}$$

[1]For further details on analytical solutions of this kind of PDEs, see [6].

[2]Functions `besselj` and `bessely` in MATLAB, see also [6].

Continuity requirements and the boundary condition give

$$G_{1,n}(r_1)x_{1,n} = G_{2,n}(r_1)x_{2,n}, \tag{28}$$

$$G_{2,n}(r_2)x_{2,n} = G_{3,n}(r_2)x_{3,n}, \tag{29}$$

$$G_{3,n}(r_3)x_{3,n} = G_{4,n}(r_3)x_{4,n}, \tag{30}$$

$$G_{4,n}(r_4)x_{4,n} = G_{5,n}(r_4)x_{5,n}, \tag{31}$$

$$\begin{bmatrix} h & -1\end{bmatrix} G_{5,n}(r_5)x_{5,n} = 0. \tag{32}$$

To obtain a bounded solution in region $i = 1$, it must hold that $b_{1,n} = 0$. Choosing $a_{1,n} = 1$, the following nonlinear equation system is obtained from the relations (28)–(32) for determining the eigenvalues λ_n

$$\begin{bmatrix} h & -1\end{bmatrix} G_{5,n}(r_5)G_{5,n}^{-1}(r_4)G_{4,n}(r_4)G_{4,n}^{-1}(r_3)\cdot G_{3,n}(r_3)G_{3,n}^{-1}(r_2)G_{2,n}(r_2)G_{2,n}^{-1}(r_1)G_{1,n}(r_1)\begin{bmatrix}1\\0\end{bmatrix} = 0. \tag{33}$$

The n:th positive root of this equation is denoted λ_n. The corresponding eigenfunction T_n is in region i described by

$$T_{i,n}(r) = a_{i,n}J_0(\mu_{i,n}r) + b_{i,n}Y_0(\mu_{i,n}r), \quad i = 1, \ldots, 5, \tag{34}$$

where $a_{i,n}$, $b_{i,n}$ can be found recursively from $a_{1,n} = 1$, $b_{1,n} = 0$ and

$$\begin{bmatrix} a_{i,n} \\ b_{i,n}\end{bmatrix} = G_{i,n}^{-1}(r_{i-1})G_{i-1,n}(r_{i-1})\begin{bmatrix} a_{i-1,n} \\ b_{i-1,n}\end{bmatrix}, \quad i = 2, \ldots, 5. \tag{35}$$

The constants d_n in (17) can be determined using the inner product defined in (21). For a unit step response in the air temperature ($T(0, R) = 1$), the following is obtained

$$d_n = \frac{\langle 1, T_n\rangle}{\langle T_n, T_n\rangle} = \frac{\sum_i \int_{I_i}(a_{i,n}J_0(\mu_{i,n}r) + b_{i,n}Y_0(\mu_{i,n}r))rc(r)\mathrm{d}r}{\sum_i \int_{I_i}(a_{i,n}J_0(\mu_{i,n}r) + b_{i,n}Y_0(\mu_{i,n}r))^2 rc(r)\mathrm{d}r}, \tag{36}$$

where I_i is the radius interval for region i and from (23)

$$\mu_{i,n} = \sqrt{\frac{c_i}{k_i}}\lambda_n. \tag{37}$$

For consistency, it is advantageous to numerically verify that the calculated eigenfunctions T_n indeed are orthogonal using the inner product defined in (21), *i.e.*,

$$\langle T_{n_1}, T_{n_2}\rangle = \int_0^R T_{n_1}(r)T_{n_2}(r)rc(r)\mathrm{d}r = 0, \quad n_1 \neq n_2. \tag{38}$$

The analytical results derived are verified with numerical simulations in Sec. VI-A. The times for computing the analytical solutions in MATLAB on a standard PC are negligible.

IV. Control System Design

The temperature stabilization is performed in multiple zones along the phase-reference line, each of an approximate width of 10 m. Thus, several control loops will be executed simultaneously. The algorithm chosen for the temperature control is based on feedback. In this context, this principle

means that the temperature is measured at selected points along the phase-reference line and the measurements are used for online computation of the amount of heat to be added using the heating cables. The control law for computing the control input u in Fig. 2 was chosen as a PID controller [7]

$$u(t) = K\left(e(t) + \frac{1}{T_i}\int_0^t e(\tau)\mathrm{d}\tau + T_d\frac{\mathrm{d}e(t)}{\mathrm{d}t}\right), \qquad (39)$$

where $e(t) = T_{\mathrm{ref}} - T$ is the control error with respect to the desired reference temperature T_{ref}. A model-based control design was pursued in order to determine the controller coefficients K, T_i, and T_d. Based on the simulations of the dynamic models established in Sec. III, which will be detailed in Sec. VI-A, the system dynamics from control input u to the temperature T can be determined to be of first order (see the relation defined in (44)) on the format

$$G_{cc}(s) = \frac{K_p}{sT_p + 1}, \qquad (40)$$

where K_p is the process gain and T_p is the time constant. The desired characteristic polynomial of the closed-loop system in the Laplace domain is parametrized as

$$s^2 + 2\zeta\omega s + \omega^2, \qquad (41)$$

where ζ corresponds to the damping and ω the speed of the resulting closed-loop system. Since the system dynamics are of first order, a PI controller, *i.e.*, $T_d = 0$, is sufficient for arbitrary placement of the poles. Pole placement [7] gives the desired coefficients of the PI controller as:

$$K = \frac{2T_p\zeta\omega - 1}{K_p}, \quad T_i = \frac{2T_p\zeta\omega - 1}{T_p\omega^2}, \qquad (42)$$

which are dependent on the system model parameters in (40). Since only heating is possible with the heating cables, the actuated control signal is saturated from below at 0.

V. Control Architecture and Prototype Setup

Various control architectures can be considered for realization of the temperature control strategy in Sec. IV. The hardware components required for the feedback control are as follows. Sensors measuring the surface temperature of the outer copper conductor are needed. Pt100 sensors of resistance temperature detector (RTD) type were chosen as the primary sensor model. Resistance wires wound around the outer copper conductor were used as heating elements. I/O:s for the signals from the sensors as well as pulse-width modulated (PWM) signals to the actuators (*i.e.*, to the heating elements) were required for a digital controller implementation. The PWM signals were fed to solid-state relays (SSRs) for power control of the heating elements. A computer or microprocessor for executing the controller algorithm in a digital implementation was also required.

A. Hardware Components and Controller Implementation

Two different solutions for the control-hardware architecture were considered. One alternative was to use Eurotherm Mini8 [8], in which up to eight PID feedback loops can be executed simultaneously. The second alternative was to use EtherCAT components from Beckhoff Automation [9]. The PID control loops were then executed inside the central accelerator control system, running the Experimental Physics and Industrial Control System (EPICS) framework [1]. The required alarm and safety functionality should be implemented in EPICS, irrespectively of the selected hardware solution. The complete control architecture with components from Beckhoff is schematically visualized in Fig. 5.

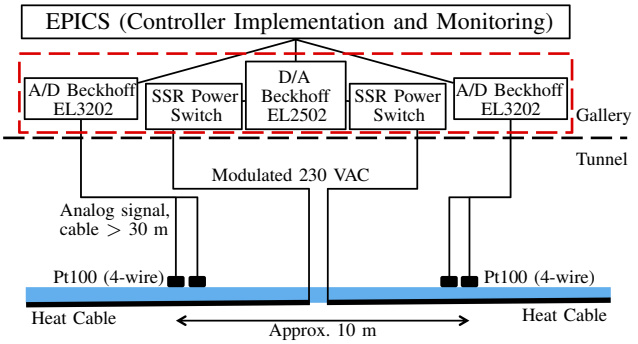

Fig. 5. Control architecture based on EtherCAT components from Beckhoff Automation. Considering the radiation expected in the accelerator tunnel, all hardware for the temperature control system will be located in the gallery outside the tunnel itself. The controller is distributed, and each temperature zone along the phase-reference line is controlled using one feedback loop.

A PID controller implementation was made in EPICS for evaluation of performance and robustness. The controller was first implemented in the Python language and later in the EPICS state-machine language by ESS. The implementation employed the inputs (temperature sensors) and outputs (relay signals) in the Beckhoff EtherCAT or Eurotherm Mini8 components. The implemented controllers comprised input-signal filtering (determined by a time constant T_f) and anti-windup functionality using the tracking method [7].

B. Prototype Setup

In the prototype setup, the layout of the phase-reference line was as follows. First, one section of coaxial line was connected to a directional coupler. Then, four consecutive sections of coaxial line were connected. Finally, one additional directional coupler was attached followed by one section of coaxial line. Each section of the coaxial line was 700 mm. Surface-mounted temperature sensors were attached on the mid-part of each section of the outer conductors of the coaxial lines as well as on the directional couplers. Consequently, eight sensors were measuring the temperature along the experimental setup. Heating cables and insulation were also mounted. A schematic description of the prototype setup with regard to sensor placement is shown in Fig. 6. The quantity used for the feedback control was the arithmetic mean of Sensors 3 and 6. For measurements of the ambient air temperature, three surface-mounted temperature sensors were attached on the outer boundary of the insulation tubes and the sensors were distributed equally along the rigid line. In the setup, heating cables with shielding and custom-made cable insulation for radiation resistance were used. A photo of the experimental setup is shown in Fig. 7.

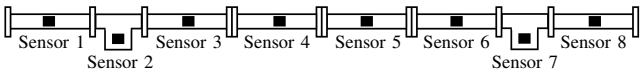

Fig. 6. Distribution of the temperature sensors in the prototype setup of the temperature control system for the phase-reference line, comprising six sections of the coaxial line, each of length 700 mm, and two directional couplers (Sensors 2 and 7). The arithmetic mean of Sensors 3 and 6 was used for the feedback control and the remaining sensors were out-of-loop used for verification of the temperature stability.

VI. Results

In this section, results from simulations as well as experiments on the prototype setup are presented. First, results from the numerical and analytical solution of the heat-transfer PDE are illustrated. Second, results from experiments where the ambient air temperature was varied are presented.

A. Simulation Results

A two-dimensional model of the cross section of the system was implemented in COMSOL Multiphysics. COMSOL employs FEM analysis [10] for numerically solving the involved PDE for heat transfer to compute the temperature distribution in the phase-reference line with insulation and applied heat using the resistance cables. The model consists of two copper conductors, with air inside the inner one and between both of them. The outer copper tube is fully covered with insulation (Fig. 3), having a thickness of 40 mm.

1) Stationary Solution: A simulation study was performed, where the initial temperature of the phase-reference line was 25 °C and the ambient temperature was held fixed at T_{air} = 25 °C. Internal RF losses in the copper tubes, leading to heat generation, were introduced according to numbers in data sheets of rigid lines of the same dimensions as the prototype setup, and the heat losses were distributed equally between the inner and the outer conductor. The results of the simulation—*i.e.*, the stationary temperature distribution under the assumed heat generation—are shown in Fig. 8.

2) Model of Disturbance Dynamics: In order to investigate the disturbance dynamics from the air temperature to the copper tube temperature, *i.e.*, $G_{ca}(s)$, a step response in T from the ambient temperature T_{air} was computed numerically using COMSOL. In addition, the obtained solution

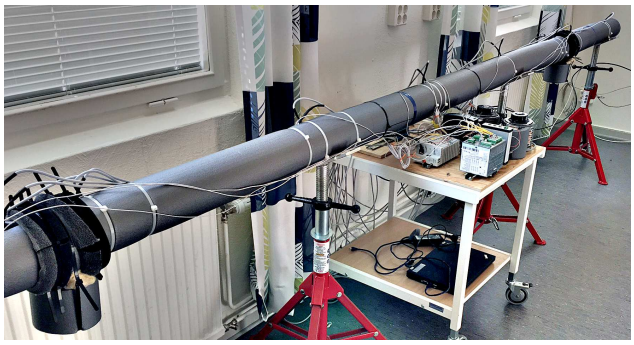

Fig. 7. The prototype setup of the temperature control system for the phase-reference line, with three sensors measuring the ambient air temperature.

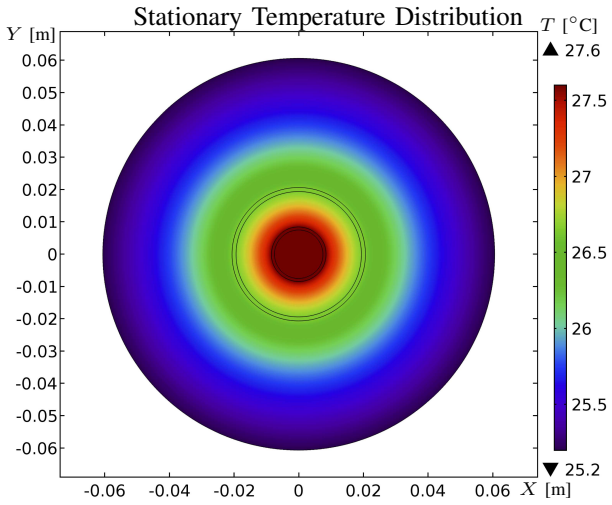

Fig. 8. Numerical simulation results obtained with constant ambient temperature (T_{air} = 25 °C) and internal heat losses (0.38 W/m) in the copper conductors. In this simulation, no additional heat was applied with the heating cables wound around the coaxial rigid line.

when numerically solving the PDE was compared to the corresponding analytic solution derived in Sec. III-D.

A transfer function was fitted to the obtained data for temperature versus time. A second-order model with a time-delay was found to be sufficient to very accurately model the dynamics. The model obtained can be stated as

$$\frac{T_{\text{cu}}(s)}{T_{\text{air}}(s)} = G_{ca}(s) = \frac{e^{-200s}}{(400s+1)(4200s+1)}, \tag{43}$$

where $T_{\text{cu}}(s)$ and $T_{\text{air}}(s)$ are the Laplace transforms of the temperature of the outer copper coaxial conductor and the air temperature, respectively.

To further investigate the dynamics of the system, the temperature distribution as function of the radius of the cross section of the phase-reference line was also computed. The simulated experiment was such that the temperature of the ambient air was increased with 1 °C, and subsequently the response of the temperature of the phase-reference line was studied. Initially, the phase-reference line had the same temperature as the ambient air. The results of the simulation are visualized in Fig. 9. The abscissa denotes the radial distance from the center of the phase-reference line. The corresponding analytic solution derived in Sec. III-D is also shown. It is clear that there is excellent agreement between the numerical simulation and the analytical solution.

3) Model of Heat Dynamics: The heat dynamics $G_{cc}(s)$ was also evaluated using simulation in COMSOL. A step response was thereby performed, *i.e.*, a constant heat source of 1 W/m was assumed on the outer copper conductor. It was around this conductor that the heating cables were uniformly wound. This assumption means that no explicit modeling of the heating cables was introduced in the model, rather a uniform heat addition was assumed. The response in temperature at the same conductor was then simulated.

A transfer-function model of first order was found to

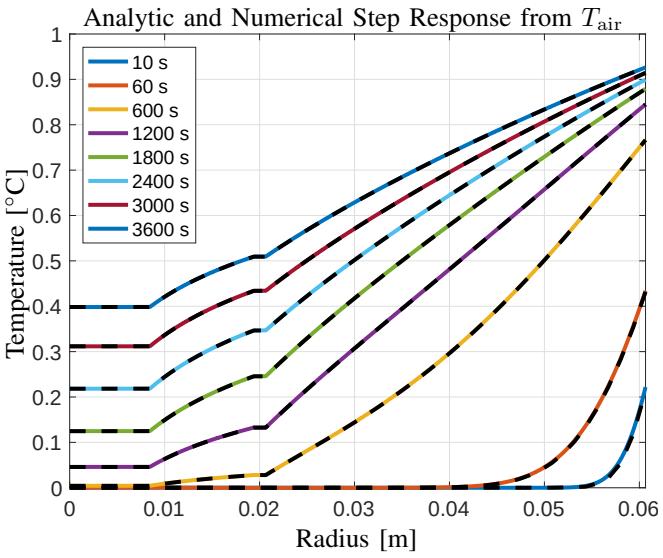

Fig. 9. Simulation results (color) for the response in temperature in the cross section from a step increase of the ambient air temperature T_{air} with 1 °C. After one hour, the temperature of the outer copper tube at $r = 0.02$ m of the coaxial line has increased approximately 0.5 °C. After 20 min, the temperature gradient in the insulation is close to linear. Also note the perfect agreement between the numerical simulations (dashed black) from COMSOL and the corresponding analytical solution from Sec. III-D.

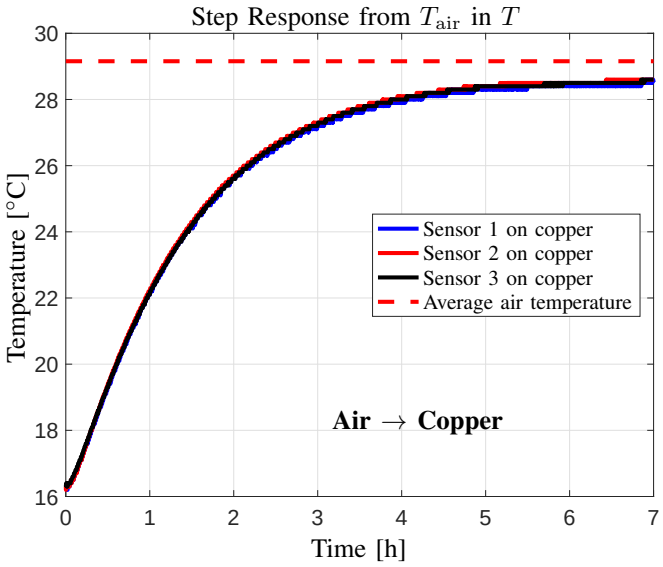

Fig. 10. Experimental results obtained as the response in T from a step change in T_{air}, performed on an initial prototype setup. The three temperature sensors were distributed equally along the copper coaxial line.

describe the dynamics of $G_{cc}(s)$ very well. The transfer-function model can be written as (in the unit °C/(W/m))

$$\frac{T_{\text{cu}}(s)}{U(s)} = G_{cc}(s) = \frac{4.29}{3800s + 1}, \tag{44}$$

where $U(s)$ is the Laplace transform of the heating signal.

B. Experimental Results

In this section, experimental results from the prototype setup are presented and analyzed regarding the requirements.

1) Results for Modeling: To the purpose of verification of the models of the heat dynamics established based on simulated data in Sec. VI-A, experiments were performed on an initial prototype of the setup described in Sec. V. The results from a step change in the temperature of the ambient air are shown in Fig. 10. The experiment was performed such that a room was pre-heated and when the temperature was stable, the prototype setup was moved into the heated room. The obtained results exhibit good agreement with the simulated data, compare in particular the time constants in the transfer function (43) and Fig. 10.

Moreover, a step-response experiment in the heating control signal u was performed. The time constant was estimated to $T_p = 3800$ s, which is in excellent agreement with the simulation, see the transfer function (44). The static gain depends on the mass of the end flanges of the phase-reference line as well as the properties of the heat transfer at the ends of the line (for obvious reasons, the insulation is not perfect). In the simulation model, infinite length of the rigid line was assumed, which means that boundary effects of this kind are not accounted for in the simulations.

2) Temperature Stabilization Results: Extensive experiments were performed on the prototype setup for evaluating the performance and robustness of the temperature-stabilization approach. On the experimental setup, a single feedback control loop was used to investigate the obtained temperature stability. The room where the setup was located was heated with an element with variable power level, while the control system for the temperature stabilization adjusted the power level in the heating cables to keep the temperature of the phase-reference line stable. The heating element contained a fan that spread the heat in the room. Therefore, the heating element was directed oppositely to the setup and the heat propagated slowly and evenly around the insulated coaxial line. The reference value for the control system was selected as T_{ref} = 30 °C. A fundamental property of the control system is that this reference must be higher than the expected maximum ambient air temperature, since only heating can be applied to the coaxial line with the heating cables. The peak-to-peak value of the variations in the ambient air temperature was tuned by adjusting the power level of the heating element. The results from one representative experiment are visualized in Figs. 11–12.

It is clear that the temperatures measured by Sensors 2–7 along the phase-reference line exhibit variations within T_{cal}±0.1 °C, where T_{cal} is the temperature at the particular measurement point at the start of the experiment (corresponding to the temperature at the calibration time). This requirement also holds for the out-of-loop sensors, which are not used for the feedback control. The results should be compared with the requirements in (1) and (2). The temperatures of the directional couplers (Sensors 2 and 7) are remarkably stable, despite that these are controlled using the same PID controller loop as the rigid coaxial line sections. Moreover, the absolute temperatures toward the flanges of the

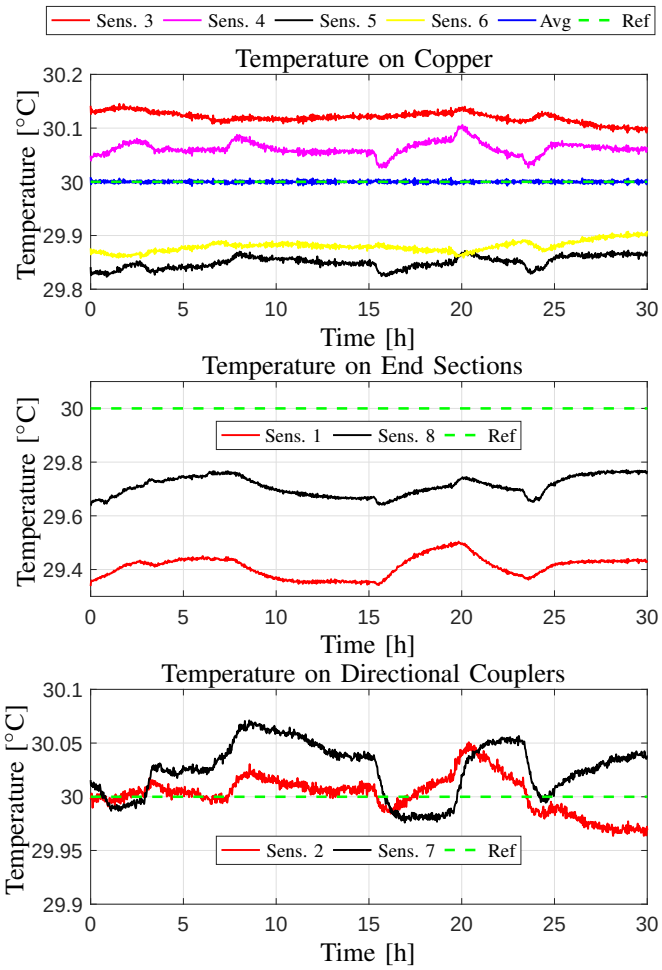

Fig. 11. Experimental results from the prototype setup, where variations in the ambient air temperature resulted from heating of the room. The arithmetic mean of Sensors 3 and 6 was used for the feedback control. Refer to Fig. 6 for a description of the placement of the different sensors. All measurements from Sensors 2–7 are within the requirement on a temperature variation of $T_{\mathrm{cal}} \pm 0.1$ °C, where T_{cal} is the temperature at the respective measurement point when the experiment starts.

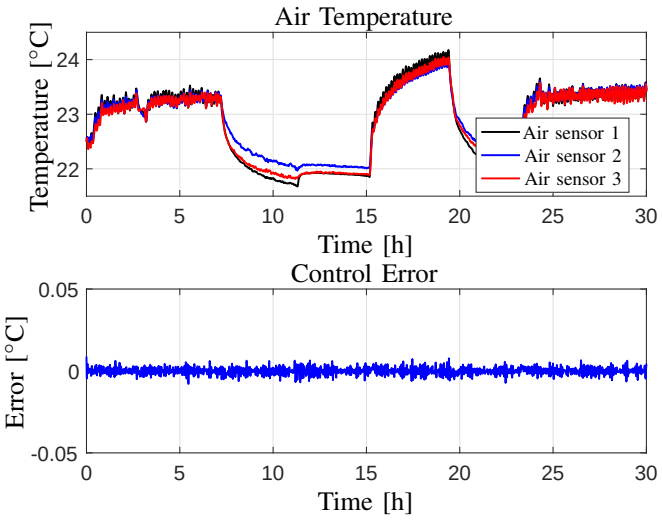

Fig. 12. Experimental results from the prototype setup, where variations in the ambient air temperature were introduced by intermittently heating the room. The measured temperatures along the prototype phase-reference line corresponding to these plots are visualized in Fig. 11.

end coaxial-line sections (Sensors 1 and 8) are slightly lower than the reference temperature and exhibit slightly larger variations. The small differences are, however, not significant as long as the variations are limited, since it is changes in temperature rather than the absolute temperature that are of importance for the stability of the phase as detailed in Sec. II.

VII. Conclusions

Based on a thorough theoretical modeling and analysis, a prototype control system and a hardware architecture for temperature stabilization of the phase-reference line at ESS were developed. The experimental results obtained from a prototype setup showed that the specification in terms of temperature deviations from the initial calibration temperatures can indeed be met (see Sec. II), despite significant disturbances by variations in the ambient air temperature. At the points along the line where measurements were acquired for the feedback control, the accuracy is approximately one order of magnitude higher than the specification. Considering the out-of-loop sensors, they, as expected, indicated slightly larger variations. This was noticed for the end sections toward the flanges of the line. This behavior will, however, most certainly be less pronounced when scaling up the control solution to the full 600 m phase-reference line at ESS, where the dynamics at the boundaries are less significant.

Acknowledgments

The authors would like to acknowledge Dr. Krzysztof Czuba and co-workers in the group at Warsaw University of Technology, who will do up-scaling of the temperature-stabilization solution and the construction work for installation of the complete phase-reference line at ESS, for interesting discussions and a smooth hand-over process of the prototype developed and the results obtained in this paper.

References

[1] S. Peggs (Ed.), "ESS Technical Design Report," European Spallation Source, Tech. Rep. ESS-doc-274, 2013, ISBN 978-91-980173-2-8.
[2] R. Zeng, "Technical appendix for phase reference distribution system," European Spallation Source, Tech. Rep., 2015, ver. 1.2.
[3] C. Piller, "SNS LLRF Reference System," Presentation slides from Oct. 12, 2005, Oak Ridge National Laboratory, Oak Ridge, TN.
[4] B. Olofsson, B. Bernhardsson, R. Zeng, and P. Andersson, "Temperature Control of the ESS Phase Reference Line," 2017, Poster at the 8th Int. Particle Accelerator Conf., Copenhagen, DK.
[5] J. H. Lienhard IV and J. H. Lienhard V, *A Heat Transfer Textbook*, 4th ed. Cambridge, MA: Phlogiston Press, 2015.
[6] G. Sparr and A. Sparr, *Kontinuerliga System*. Lund, Sweden: Studentlitteratur, 2000.
[7] K. J. Åström and T. Hägglund, *Advanced PID Control*. Research Triangle Park, NC: ISA—The Instrumentation, Systems and Automation Society, 2006.
[8] Eurotherm Mini8, Accessed: 2017-12-25. [Online]. Available: https://www.eurotherm.se/products/temperature-controllers/multi-loop/mini8.
[9] Beckhoff Automation, Accessed: 2017-12-25. [Online]. Available: https://www.beckhoff.de.
[10] N. S. Ottosen and H. Petersson, *Introduction to the Finite Element Method*. Upper Saddle River, NJ: Prentice Hall, 1992.